An Internal Fractional Boundary Placement Model for the Transmission-Line Modeling Method

Mark Panitz and Christos Christopoulos

George Green Institute for Electromagnetic Research
School of Electrical and Electronic Engineering
University of Nottingham, Nottingham, NG7 2RD, United Kingdom
christos.christopoulos@nottingham.ac.uk

Abstract ─ This paper describes a fractional boundary placement model for the transmission-line modeling method enabling the positioning of internal boundaries at non-integer cell locations. The model does not introduce any restriction on the maximum timestep of simulations. The connection of the boundary model to a regular mesh is shown and the model is validated using a band-pass waveguide filter model. Results show good agreement with the analytical solution for the waveguide problem.

Index Terms ─ Full-field electromagnetic modeling, time domain analysis, transmission-line matrix methods, waveguide.

I. INTRODUCTION

In its simplest form, the transmission-line modeling method, or matrix method, (TLM) requires space to be discretized into uniform cells of equal size [1]. The most commonly used TLM cell in three dimensions (3D) is the symmetrically condensed node (SCN), a twelve port transmission-line junction which models both electric and magnetic field components at the node centre. The modeling approach applies the equivalence of Maxwell's curl equations to the telegrapher's equations where

$$\underline{E} = -\frac{V}{\Delta l}, \quad \underline{H} = -\frac{I}{\Delta l}. \qquad (1)$$

Space is discretized using such nodes, which are then solved in an explicit manner through a two stage scatter-connect approach. Therefore, the timestep of the simulation is chosen to maintain synchronization throughout the mesh and is determined by the smallest cell size. Unlike some other numerical techniques, the TLM algorithm does not involve any convergence criteria, a property that makes it an inherently stable method [2].

In an uniform SCN mesh all cells are the same size but graded mesh formulations do exist and offer geometrical flexibility [1]. The grading of the mesh determines the smallest cell size and hence the timestep that must be used in the simulation. Typically, the smaller the cell size the smaller the timestep must be.

Perfect electric conductor (PEC) boundaries in the standard TLM method are usually realized by positioning them at cell faces. Hence, boundaries must be positioned at mesh lines within the model. The PEC boundary condition is applied in the connection stage by setting the reflected voltage, from the boundary, to be the negative of the incident voltage.

To accurately model geometry, it is often necessary to arbitrarily position object boundaries within the mesh. The structured mesh may not offer enough flexibility to conform to the model geometry and a higher mesh density or a graded mesh must be used. In both cases, the simulation timestep must be reduced, increasing the total CPU time for the problem. To maintain synchronization and stability, the maximum time step that can be used in the standard 3D TLM method is

$$\Delta t_{\max} = \frac{\Delta l_{\min}}{2c}, \qquad (2)$$

where Δl_{min} is the smallest cell edge length in the mesh.

A fractional external boundary placement model was developed in [3] where space between an arbitrarily positioned boundary and a structured mesh is modeled by a transmission-line parallel to the boundary. This approach allows the boundaries around cavity type problems to be positioned anywhere within a cell without limiting the timestep used. Here, external refers to the modeling domain, which is the boundary where the modeling space is truncated.

In order to model a general problem where structure is contained within the body of the mesh, for example a waveguide aperture problem or large scale EMC type problem, internal boundaries must be modeled. This requires the correct treatment of fields on both sides of the boundary and along the laminae edge of the boundary, such as around an aperture.

This paper extends the model in [3] to internal boundaries so that objects within the modeling domain can be positioned in an arbitrary manner without modifying the structure of the rest of the mesh. This is done without introducing restriction upon the simulation timestep.

II. TWO DIMENSIONAL FORMULATION

The boundary model is developed initially in two dimensions (2D) in order to reduce the complexity of the formulation. Extension to three dimensions is straightforward and is described in Section III. In 2D, the model will be derived to be coupled to the 2D TLM series node [1]. The series node is formed from four transmission-lines connected at a junction in a series manner.

The aim is to replace the 2D series node by a structure that models the field propagation due to a boundary positioned within the cell. The 2D series node is therefore replaced by the construction shown in Fig. 1 where, in this case, the boundary is positioned along the x-axis. A single boundary cell is present in the mesh and the connecting transmission-lines of the adjacent cell can be seen. Although the 2D node only has four ports, the port numberings are chosen to be consistent with the 3D SCN.

The boundary model is a time-domain implementation of the circuit shown in Fig. 1 which is a 1D transmission-line segment running parallel to the boundary. The boundary properties will be modeled by the inductance and capacitance

of the transmission-lines. Coupling of the boundary model to the 2D series nodes is performed through the voltage sources on the transmission-lines and coupling to the boundary end through a potential divider.

Here, only cases where the skin depth is small compared to the boundary thickness are considered. Hence, it is assumed that there is no propagation across the boundary and it is a perfect electric conductor (PEC).
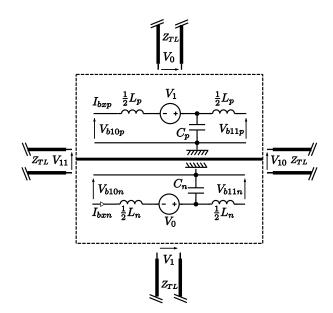

Fig. 1. 2D internal fractional boundary cell - port numbering is consistent with the 3D symmetrically condensed node (SCN).

A. Boundary properties

The two regions of space on either side of the boundary are designated the subscripts n and p, that is the region which has its normal facing negatively and positively with respect to the coordinate system.

The thickness of the boundary is given by h and the displacement of the boundary from the cell face is given by d so that

$$d_p + d_n + h = \Delta l, \qquad (3)$$

where Δl is the cell spacing. Therefore, for a laminae boundary, the value of h is zero and for a real boundary with thickness the value of h is in the range $0 < h < \Delta l$. In order to model a boundary with thickness greater than Δl, the modeller must construct the boundary in more than a single plane of cells, in the same manner as would usually be applied in these cases.

The formulation proceeds from the one dimensional telegrapher's equations where, for the positive side of the boundary;

$$-\Delta l \frac{\partial V_{bp}}{\partial x} = L_p \frac{\partial I_{bxp}}{\partial t} - V_1, \qquad (4)$$

$$-\Delta l \frac{\partial I_{bxp}}{\partial x} = C_p \frac{\partial V_{bp}}{\partial t}. \qquad (5)$$

The per-unit-length capacitance and inductance and characteristic impedance are determined by the volume of space adjacent to the boundary. The capacitance and inductance not modeled by the transmission-lines themselves will be modeled by the transmission-line stubs [1]. The per-unit-length capacitance and inductance and characteristic impedance that are to be modeled by the boundary model are

$$C_p = \frac{C}{\Delta l} = \frac{\varepsilon_0 \Delta l}{d_p}, \qquad (6)$$

$$L_p = \frac{L}{\Delta l} = \frac{\mu_0 d_p}{\Delta l} \qquad (7)$$

and

$$Z_{bp} = \sqrt{L_p / C_p} = \eta_0 \left(\frac{d_p}{\Delta l} \right). \qquad (8)$$

Converting equations (4) and (5) to travelling wave format [3, 4] yields the boundary voltage and current expressions

$$V_{bp} = \frac{\left(V_{b10p}^i + V_{b11p}^i + V_{bCp}^i \right)}{\sqrt{2}}, \qquad (9)$$

$$I_{bxp} = \frac{\left(V_{b10p}^i - V_{b11p}^i - V_{bLpx}^i + \frac{1}{2} V_1 \right)}{\sqrt{2} Z_{bp}}. \qquad (10)$$

In (10), the voltage coupled from the bulk mesh is given by

$$V_1 = 2V_0^r - I_{bxp} Z_{TL}, \qquad (11)$$

where V_0^r is the reflected port voltage on the series node coupling to the boundary model.

The stub impedances are expressed here in terms of Z_{bp} and have been obtained in the same manner as in [3] where speed of light propagation along the transmission-line is required. This requires the introduction of the stubs to model additional capacitance and inductance within the boundary model. These expressions define the TLM equivalent circuit of the boundary model

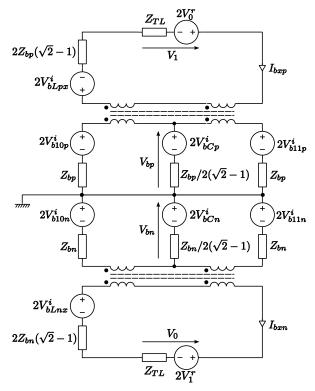which is shown in Fig. 2 for both sides of the boundary.

Fig. 2. Thevenin equivalent circuit of the 2D internal fractional boundary model - port numbering is consistent with the 3D symmetrically condensed node (SCN).

B. Boundary update

The boundary model is updated during the connection stage of the TLM algorithm. Therefore, the boundary model uses the reflected voltage from the adjoining cell as its inputs. Following scattering throughout the mesh, the voltage and current in the boundary cells are calculated using equations (9) and (10). The boundary scatter then proceeds by calculating the voltages reflected along the boundary length given by

$$V_{b10p}^r = V_{bp} - I_{bxp} Z_{bp} - V_{b10p}^i \qquad (12)$$

and

$$V_{b11p}^r = V_{bp} + I_{bxp} Z_{bp} - V_{b11p}^i. \qquad (13)$$

The stub voltages are updated for the next timestep in the usual way so that for the inductive stub

$$_{k+1}V_{bLpx}^i = -\left(_k V_{bLpx}^i + 2\left(\sqrt{2} - 1 \right) I_{bxp} Z_{bp} \right) \qquad (14)$$

and for the capacitive stub

$$_{k+1}V^i_{bCp} = V_{bp} - {}_kV^i_{bCp}. \qquad (15)$$

These expressions complete the update of voltages within the boundary model. Connection must also be made to the nodes of the bulk mesh adjacent to the boundary nodes, which is described in the following subsection.

C. Boundary connection

Three types of connection must take place in the boundary model: connection along the boundary, connection to the mesh normal to the boundary, and connection to the mesh at the ends of the boundary.

Connection along the length of the boundary is performed by calculating the total voltage at the connecting ports. Connection of the nth boundary node to the $(n+1)^{th}$ boundary node would yield a total voltage of

$$V_{b11,10p} = \Big(2\,{}_kV^r_{b11p}(n)Z_{bp}(n+1) +$$
$$2\,{}_kV^r_{b10p}(n+1)Z_{bp}(n)\Big)/ \qquad (16)$$
$$\Big(Z_{bp}(n) + Z_{bp}(n+1)\Big)$$

and hence, the incident voltages at the next timestep are given by

$$_{k+1}V^i_{b11p}(n) = V_{b11,10p} - {}_kV^r_{b11p}(n) \qquad (17)$$

and

$$_{k+1}V^i_{b10p}(n+1) = V_{b11,10p} - {}_kV^r_{b10p}(n+1). \qquad (18)$$

This connection procedure allows the boundary displacement or thickness to vary between boundary cells and ensures conservation of energy as a result of these variations.

Connection to the bulk mesh normal to boundary is simply carried out through the voltage source on the boundary transmission-line. The mesh is updated using the expression

$$_{k+1}V^i_0 = {}_kV^r_0 - {}_kI_{bxp}Z_{TL}. \qquad (19)$$

Finally, connection to the edge of the boundary is performed by calculating the loop current at the boundary end given by

$$_kI_{b10,11} = \frac{-2\big({}_kV^r_{b10p} + {}_kV^r_{b10n}\big) + 2\,{}_kV^r_{11}}{Z_{TL} + Z_{bp} + Z_{bn}}, \qquad (20)$$

where $_kI_{b10,11}$ denotes the current loop due to the boundary ports *10p* and *10n* and the regular TLM port *11*. The reflected port currents are then given by

$$_{k+1}V^i_{11} = {}_kV^r_{11} - {}_kI_{b10,11}Z_{TL}, \qquad (21)$$

$$_{k+1}V^i_{b10p} = {}_kV^r_{b10p} + {}_kI_{b10,11}Z_{bp}, \qquad (22)$$

and

$$_{k+1}V^i_{b10n} = {}_kV^r_{b10n} + {}_kI_{b10,11}Z_{bn}. \qquad (23)$$

These expressions form a potential divider circuit at the boundary edge to ensure that the incident field is split between either side of the boundary in the correct manner. These expressions complete the boundary to bulk mesh updates and provide the incident voltages for the next iteration of the model.

III. EXTENSION TO THREE DIMENSIONS

The internal boundary model has been defined in 2D based on the series TLM node. Extension to three dimensions (3D) is realised by modeling the boundary as a 2D shunt grid adjacent to the boundary, rather than the 1D line used for the 2D model.

Following the same procedure as in 2D and starting from the telegrapher's equations for the 2D shunt grid:

$$-\Delta l \frac{\partial V_{bp}}{\partial x} = L_p \frac{\partial I_{bxp}}{\partial t} - V_1, \qquad (24)$$

$$-\Delta l \frac{\partial V_{bp}}{\partial y} = L_p \frac{\partial I_{byp}}{\partial t} - V_7, \qquad (25)$$

and

$$-\Delta l \frac{\partial I_{bxp}}{\partial x} - \Delta l \frac{\partial I_{byp}}{\partial y} = C_p \frac{\partial V_{bp}}{\partial t}, \qquad (26)$$

yields the circuit equivalent equations that are to be solved. The boundary impedance remains the same as in 2D and is given by (8) and the update equations are given

$$V_{bp} = \frac{\big(V^i_{b8p} + V^i_{b9p} + V^i_{b10p} + V^i_{b11p}\big)}{4}, \qquad (27)$$

$$I_{bxp} = \frac{\big(V^i_{b10p} - V^i_{b11p} - V^i_{bLpx} + \frac{1}{2}V_1\big)}{4Z_{bp}}, \qquad (28)$$

and

$$I_{byp} = \frac{\big(V^i_{b8p} - V^i_{b9p} - V^i_{bLpy} + \frac{1}{2}V_7\big)}{4Z_{bp}}. \qquad (29)$$

In the 3D case, there is no capacitive stub as all the required capacitance is modeled by the link lines.

The link line voltages are scattered in the same manner as in (12) and (13) and the stub voltage is updated as in (14), where in this case the inductive stub impedance is simply $2Z_{bp}$.

A. Boundary connection

The boundary connection in 3D is performed in the same manner as in 2D. At each connecting port, the total field is calculated and the reflected field is then obtained and is dependent on the displacement and thickness of the boundary. When connecting the boundary edge to the 3D SCN, the coupling requires treatment of the voltage port that does not have a corresponding boundary port, such as port V_5 as shown in Fig. 3.
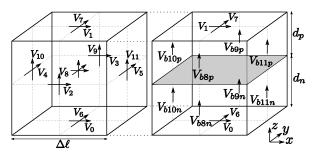

Fig. 3. Port numberings of the 3D boundary model (right) and a connecting adjacent SCN (left) showing the unmatched SCN port (V_5).

Connection of the other port, normal to the boundary, is performed in the same way as in 2D. The total field is calculated and the reflected voltages are then obtained. In the case of a boundary in the x-y plane as shown in Fig. 3, the electric field polarised normal to the boundary is assumed to be continuous at the boundary edge, permitting direct connection between the two regions. The unmatched port of the SCN (V_5) is polarised in the plane of the boundary however.

The boundary displacement must be less than the cell it is within, hence less than Δl. Furthermore, as a rule of thumb, the mesh cell size, Δl, should be smaller than one-tenth of the wavelength of interest to provide suitable accuracy and reduce dispersion [1]. Hence, it is assumed that the field polarised in the plane of the boundary in the region adjacent to the boundary is zero. This component is not modeled by the boundary model, and furthermore, this assumption implies that the field polarised parallel to and incident upon the edge to the

boundary plate sees a PEC boundary condition. Hence, this port of the SCN is updated through

$$_{k+1}V_5^i = -\,_kV_5^r, \tag{30}$$

in the same manner as the PEC boundary condition is usually applied to the SCN cell.

IV. COMPUTATIONAL PERFORMANCE

The computational performance of this numerical method is assessed with respect to the scattering process within a free-space series node in 2D and the free-space SCN node in 3D. The rationale for this is that the internal boundary model described here replaces the whole TLM cell and, although solved during the connection process, the update of the internal boundary cell can be considered an equivalent scattering process for the cell.

The computational requirements of the boundary model with the normalised free-space TLM cell are compared for 2D in Table 1 and in 3D in Table 2, where for the free-space cells the circuit based algorithm described in [4] is used.

Table 1: Comparison of the computational requirements of the free-space series node and the internal boundary node in 2D

	Free-space	Boundary
Variables	4	12
Calculations	7	14

Table 2: Comparison of the computational requirements of the free-space SCN and the internal boundary node in 3D

	Free-space	Boundary
Variables	12	18
Calculations	18	22

An expected increase in variables and computations can be seen for the boundary cells. However, it is not expected that this increase will affect the computational performance of the full TLM model greatly as the number of boundary cells would be only a small fraction of the total cells in the simulation model.

The most significant computational advantage of this procedure is that no modification of the simulation timestep is required to accommodate the boundary displacement. The transmission-line

impedances are determined by the offset of the boundary from the cell edges as in (8). It can be seen that all transmission-line impedances for the link lines and stubs are positive for all positive displacements. Hence, there is no restriction to the simulation timestep necessary to maintain stability of the model as is required in a graded approach. Even as the boundary displacement tends to zero the simulation timestep can still be maintained at the maximum of the bulk mesh. Hence, any value of h in the limit $0 < h < \Delta l$ and d in the limit $0 < d < \Delta l$ can be used providing (3) is satisfied without a reduction in timestep.

Furthermore, as the timestep is not affected by the introduction of the boundary model it is not necessary to load the bulk mesh with stubs to adjust its timestep, as required in a graded mesh. Therefore, this model avoids the unwanted dispersion effects of the stub loaded TLM mesh [1] giving improved model accuracy over graded approaches.

V. VALIDATION

Validation of the boundary model addresses the two parts of the algorithm: the displacement of the boundary within the cell and the connection of the boundary to the surrounding mesh.

Regarding the displacement of the boundary, the accuracy of the external boundary model is determined in detail in [3] it is shown that the propagation velocity and boundary displacement have errors of only 0.00003% and 0.01%, respectively. The displacement model used here is based on the same procedure as that in [3], therefore the errors in the propagation velocity and boundary displacement will be identical to that of the external boundary.

To validate the model in this paper, it must be ensured that the procedure used to couple the ends of the boundary to the regular mesh is valid and that the displacement model functions correctly on both sides of the boundary. The validation is performed using a waveguide band-pass filter model in the following subsection.

A. Waveguide band-pass filter

The boundary model developed here takes into account two modes of connection to the bulk mesh, that is perpendicular and normal to the boundary. Here, this model is validated using a case requiring

use of both the displacement and connection of the boundary model.

A waveguide filter within a WR-28 ($f_c =$ 31GHz) waveguide is chosen consisting of four inductive apertures with periodic separation. A schematic of the structure is shown in Fig. 4. where the H_{10} (TE_{10}) mode is excited so that the electric field is orientated vertically in the waveguide.

Fractional boundaries

$a = 7.11\text{mm} = 11\Delta l$
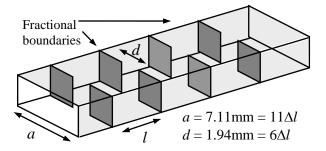$d = 1.94\text{mm} = 6\Delta l$

Fig. 4. Waveguide band-pass filter with the apertures modeled using the boundary model.

The admittance of each of the inductive apertures is given in [5] where

$$Y / Y_0 = -\left(j\lambda_g / a \right)\cot^2\left(\pi d / 2a \right). \quad (31)$$

In (31) λ_g is the guide wavelength, Y_0 is the admittance of the waveguide without the aperture and the dimensions are as labeled in Fig. 4. Hence, combining the multiple apertures shown in Fig. 4. yields an analytical reflection coefficient of

$$\cosh\left(\Gamma \right) = \cos\left(\frac{2\pi l}{\lambda_g} \right)$$
$$+ \frac{\lambda_g}{2a}\cot^2\left(\frac{\pi d}{2a} \right)\sin\left(\frac{2\pi l}{\lambda_g} \right). \quad (32)$$

In the pass-band $|\Gamma|<1$ and the reflection coefficient has no real part. The geometry is initially modeled using only the usual TLM boundary model where the aperture spacing is chosen to be an integer number of cells, so that $a =$ 7.11mm $= 11\Delta l$ and the aperture width is $d =$ 1.94mm $= 6\Delta l$. Using the standard boundary model, the aperture spacing was set to $l = 20\Delta l$ and $19\Delta l$ and the |S21| response of the filter was simulated. The H_{10} mode was propagated down the waveguide and the response was taken with and without the filter inserted.

The internal fractional boundary model was then used on the first and third apertures to model a separation of 19.5Δl, i.e. with a boundary

displacement of $0.5\Delta l$. The boundary developed here allows this case to be modeled without any change to the mesh spacing or the simulation timestep. The response of the three aperture placements are shown in Fig. 5.
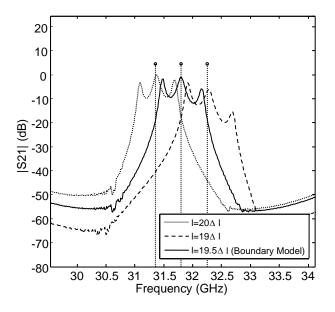

Fig. 5. |S21| response of the waveguide filter using three different aperture separations and the corresponding analytical solutions (vertical lines).

The pass-band of the waveguide filter can be easily identified in each case and the spacing of the apertures can be seen to adjust the centre frequency of the filter. The boundary model has been used to model the intermediate aperture spacing. The result shows that the model has allowed modeling of this intermediate case as the pass-band can be seen to be directly between the two extreme cases.

There is excellent agreement with the analytical solution calculated using (32) for the centre frequency of the filter, where the analytical results are shown by the vertical dotted lines terminated by small circles in Fig. 5. It was possible to obtain this numerical result without any modification of the rest of the mesh or any adjustment of the simulation timestep. This makes the model very suitable for optimisation problems where it may be necessary to modify the position of structures by small amounts between simulations.

VI. CONCLUSION

An internal boundary model for the TLM method has been developed allowing unrestricted boundary placement with no deleterious effect on the timestep. This model allows PEC structures to be positioned anywhere within a structured TLM mesh without the need for a graded mesh approach. This offers significant advantages in computational runtimes and modeling accuracy.

Coupling of the boundary to the bulk mesh has been discussed for connection both perpendicular and parallel to the boundary. Validation using a band-pass waveguide filter shows that the model allows the filter apertures to be arbitrarily and accurately positioned. The results agree well with the analytical centre frequencies of the band-pass models.

REFERENCES

[1] C. Christopoulos. *The Transmission-line Modelling Method*, Piscataway, NJ: IEEE Press, 1995.

[2] R. Ciocan, N. Ida, E. Ciocan, and H. Jiang. "Applications of the Transmission Line Matrix Method to Microwave Scanning Microscopy," *Applied Computational Electromagnetic Society (ACES) Journal*, 19(1), pp. 94-100, Mar. 2004.

[3] M. Panitz, J. Paul, and C. Christopoulos, "A Fractional Boundary Placement Model using the Transmission-Line Modelling Method," *IEEE Transactions on Microwave Theory and Techniques,* 57(3), 2009.

[4] J. Paul, *Modelling of General Electromagnetic Material Properties in TLM*, Ph.D. dissertation, School of Electrical and Electronic Engineering, The University of Nottingham, Oct. 1998.

[5] S. Ramo, J. R. Whinnery, and T. Van Duzer, *Fields and Waves in Communication Electronics.* NY: Wiley, 3rd ed, 1994.

Mark Panitz was born in Scunthorpe, U.K., in 1983. He received the M.Sci.degree in Physics from the University of Nottingham, U.K., in 2006. He received his Ph.D. in Electrical and Electronic Engineering from the University of Nottingham. U.K., in 2011. His research involved the numerical modeling and characterisation of highly reverberant, low-loss, time-varying environments with an assessment of their impact on wireless communication systems and protocols. Currently he is working with BAE Systems, U.K., as a research scientist. His research interests include Computational Electromagnetics and Electromagnetic Compatibility. He is the author of many papers in wireless propagation modeling in resonant systems and computational electromagnetic modeling.

Christos Christopoulos was born in Patras, Greece, on September 17th, 1946. He received the Diploma in Electrical and Mechanical Engineering from the National Technical University of Athens in 1969 and the M.Sc. and D.Phil. from the University of Sussex.

He is currently Professor of Electrical Engineering at the University of Nottingham. His interests include Computational Electromagnetics, Electromagnetic Compatibility and Protection of Power Networks.

He is the author of over 350 publications, seven books, and seven chapter contributions. He is a member of the IET and an IEEE Fellow. He is a past Executive Team Chairman of the IEE Professional Network in EMC and Associate Editor of the IEEE EMC Transactions.